Direct Visualization of Real-World Light Transport

Matthias B. Hullin[1] Martin Fuchs[1] Boris Ajdin[1]
Ivo Ihrke[2] Hans-Peter Seidel[1] Hendrik P. A. Lensch[1]
[1]MPI Informatik [2] University of British Columbia
Email: {hullin,mfuchs,bajdin,hpseidel,lensch}@mpi-inf.mpg.de
ivoihrke@cs.ubc.ca

Abstract

Light transport in complex scenes with possibly intricate optical properties is difficult to grasp intuitively. The study of light transport has so far mainly been conducted by indirect observations. Cameras or human observers typically only sense the radiance reflected from a scene, i.e. the light directly emitted or reflected from the last bounce of a possibly much longer light path.

Models for the propagation of light, however, typically assume light waves or rays, concepts which so far have been communicated in an abstract way using formulas or sketches. In this paper, we propose the use of fluorescent fluids for direct visualization of light transport in the real world. In the fluorescent fluid the traces of light become visible as a small fraction of the energy transported along the ray is scattered out towards the viewer. We demonstrate this visualization for direct illumination effects such as reflections and refractions at various surfaces, as well as for global effects such as subsurface light transport in translucent material, caustics, or interreflections. As this allows for the inspection of entire light paths, rather than the last scattering event, we believe that this novel visualization can help to intuitively explain the phenomena of light transport to students and experts alike.

1 Motivation

When studying light transport, students are often faced with the task of developing a solid, reliable intuition of the various interactions that can occur between light and matter. However, while light transport takes place all around us, it is hard to observe, as we only perceive its effects and not the light transport itself.

In this article we present a novel way of visualizing light transport: we propose a simple method that enables us to make light paths actually visible to the human eye. As in our recent work on Fluorescent Immersion Range Scanning [12], we modify the volume in which the light travels such that the transport itself can be observed. The observation volume is filled with a fluorescent liquid that scatters light homogeneously from any point along a ray towards the observer. As fluorescent scattering increases the wavelength of the illuminating light, the scattered (visualizing) ray does not interact with the volume again.

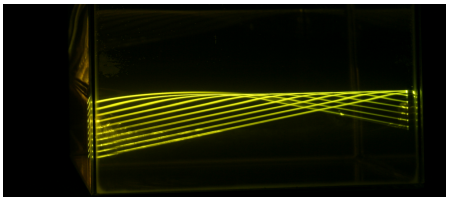

Figure 1: Visualization of a superior mirage in the extended interface layer between fluids of different index of reflection (glycerol/water mixture). By adding a fluorescent dye we make these curved light rays visible inside the real volume, creating a 3D viewing experience.

This provides a real-world view on the abstract concept of light transport as opposed to the sketches previously employed. The experience is fully three-dimensional and real-time interactive. The same method can be used to study mirror and diffuse reflections, refraction, and multi-bounce light transport. As the visualization occurs inside a 3D volume rather than by a projection onto a 2D plane complex effects such as anisotropic BRDFs, caustics, astigmatic lenses or mirages as in Figure 1 can now be inspected easily.

In the course of this article, we first shortly re-

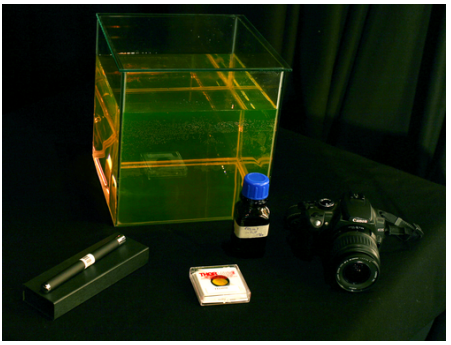

Figure 2: The equipment used for our visualization: A tank filled with water and a pinch of a fluorescent dye (Eosin Y), a laser pointer, a camera, and an optical longpass filter.

view related work and then introduce the visualization principle employed in more detail. In Sections 4, 5 and 6 we demonstrate the individual effects that can be observed. Finally, we discuss limitations and possible extensions.

2 Related Work

The light transport in a real-world scene can be rather complex, and a detailed investigation of the interplay between scene properties and light transport complexity is still at its beginning. Durand et al. [3] analyze the effect of transport, reflections, and occlusion in the frequency domain of light fields. Maharjan et al. [13], on the other hand, show how the dimensionality of the light transport within a small spatial neighborhood is linked to the bandwidth of the BRDF and the local surface curvature. Understanding the structure of light transport can help developing more efficient techniques for rendering or acquisition (e.g. [14, 5]). With our novel visualization technique we hope to provide an additional tool towards analyzing and understanding light transport.

For centuries scientists have employed ray optics to model light transport. In computer graphics, sketches of rays are frequently employed to depict the light propagation from the light source to the observer through a complex scene [20, 4, 18]. Similarly, the geometric setup of the interaction of light and matter is often shown as a ray-surface diagram, e.g. for Snell's law [4], and the resulting light distribution from complex BRDFs as collections of rays [17] or as shaded lobes [8]. Quantitative results on surface reflection are most often plotted as 1D-profiles along individual light planes [19, 16], and for anisotropic materials sometimes as orthographic views of 3D lobes [15].

The most common technique for visualizing real-world light transport is to place a diffuse 2D surface into the light path. In physics classes, for example, the effect of depth-of-field of a lens system is often demonstrated by projection onto a 2D screen at different locations. Similarly, the colored dispersion of a prism is visualized by making light rays hit the ground plane, a diffuse reflector, under a shallow angle.

In order to efficiently capture the BRDF or light distribution due to a specific material, a number of different measurement setups have been created that allow to observe the two-dimensional angular radiance distribution due to a specific illumination in a single image. One can achieve this effect by looking into a particularly shaped mirror [19, 6] or by using a diffuse sphere [10] surrounding the specimen. The image formed by these specialized reflectors allows for a direct visualization of the reflected radiance distribution. However, they require the reflection to originate from a single point on the specimen.

In our approach we make light rays visible in 3D, in an otherwise clear medium. Rather than requiring a projection surface, we use the effect of fluorescence to visualize spatial light distributions, avoiding the sometimes difficult placement of a projection plane. Furthermore, our method introduces no additional obstruction. Instead, the structure of the light transport in the scene is almost unaffected, especially compared to the possible use of scattering media that preserve the wavelength, such as smoke [11], where multiple scattering would impact the actual light transport and the observation significantly.

The use of fluorescent marker particles is common in the fluid imaging community. There, fluorescent markers are inserted into fluid flows of interest and scanned by a rapidly moving laser sheet, see e.g. the work of Deusch and Dracos [2]. In contrast, we employ a homogeneous medium and focus on static illumination effects, visualizing the spread of light.

A related example for visualizing paths of ionizing particles is the nebula or bubble chamber [7]

filled with a liquid heated to just below its boiling point. Here, the liquid vaporizes around the particle's traces, forming microscopic bubbles in the otherwise transparent chamber.

3 Visualization Principle

Just as in [12], we employ fluorescent dye as a marker for light power density. This time, however, we are not as much interested in the detection of surfaces as we are in the observation of various features of light transport. We assemble the scene constellation we want to investigate inside a transparent liquid – usually water – which contains a small concentration of Eosin Y, a fluorescent agent (see Figure 2). The exact concentration of Eosin Y is of minor importance (approx. 0.5 mg$\cdot l^{-1}$) since the appearance of the visualization hardly changes when varying its concentration by up to one order of magnitude. As a light source, we use a frequency doubled Nd:YAG laser ($P = 60\,\text{mW}$, $\lambda = 532\,\text{nm}$) and a computer controlled XY pair of galvanometer scanners. Note however, that inexpensive tools like a standard (green light) laser pointer and burst or diffraction gratings to produce ray bundles could equally well be employed.

If an Eosin molecule is hit by a photon whose wavelength lies in the absorption spectrum, it can be excited to a higher electronic state. The relaxation occurs spontaneously under emission of a photon at a longer wavelength. Due to the small overlap of the absorption and the emission spectra the liquid is virtually transparent to the emitted light. Compared to other scattering mechanisms fluorescence is typically isotropic. The scattered light can thus be observed equally well from any direction.

Additionally, due to the frequency shift inherent in the fluorescence process, an optical longpass filter (Thorlabs FEL0550) with a cut-off wavelength of $\lambda_c = 550\,\text{nm}$ can be used to block the original wavelength of the laser. This way, direct surface reflections towards the observer, which would be highly dependent on the viewing direction can be effectively filtered out, resulting in a mostly view-independent visualization of the light transport.

3.1 Image Formation Process

Even though the fluorescent dye allows for single scattering observation of light rays, resulting images of the volumetric structure will contain a few additional, sometimes unwanted effects:

1. Since the fluid is transparent to the viewing rays, each view and each captured image shows the integrated volumetric emission of light along the viewing ray. All scattering events along these rays are accumulated. While this effect is negligible when observing individual light rays it is relevant when viewing the volumetric effect of light being scattered at a surface into a cone of directions (see next section). Rather than observing a slice through the light distributions, as is common in sketch-based representations of light transport, one actually sees the integral projection of the entire lobe.
2. The second effect is caused by the isotropic fluorescent emission of the dye. As each particle along the light path emits light, all illuminating light paths themselves act as light sources inside the scene. The scattered light thus becomes visible as reflections in the scene surfaces.

   Observe, for example, the incident ray, the mirror ray, and the entire lobe being mirrored in the billiard ball in Figure 3 (glossy) and the characteristic X-shape on the mirror ball, Figure 3 (mirror). Fortunately, this illumination usually has a much lower intensity than the primary illuminating light. However, while in most cases this effect is not too disturbing it may add clutter to complex scenes with many shiny or mirroring surfaces. Additionally, it makes diffuse surfaces appear brighter then they would under laser illumination alone.
3. Solid objects will obstruct views on the light transport behind them, and transparent objects as well as the walls of the container might result in distorted views of the volumetric light distribution.

The effects described here are due to the two light paths involved in the image formation of the volumetric scene, the incident illumination light path and the viewing light path. The occasional difficulty in interpreting two-dimensional images taken this way are compensated when interactively viewing the experimental setup in three dimensions.

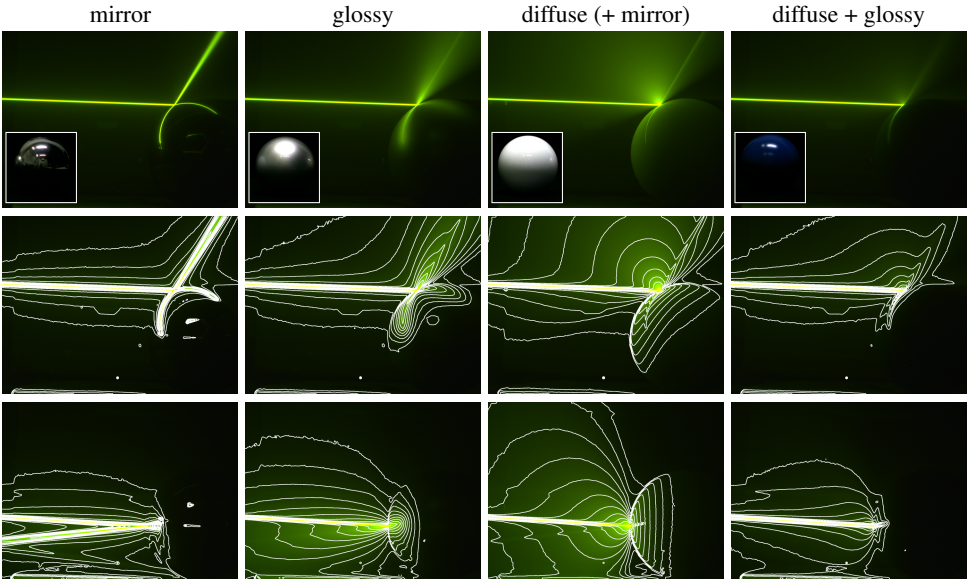

Figure 3: Light distributions reflected of various surfaces for two different incident angles.

4 Surface Properties

In this section we demonstrate the suitability of the proposed method to visualize light interaction with surfaces of general type. We show exemplary images of the major types of surface reflection: diffuse, glossy, specular and mirror reflections. We also show examples of translucent and transparent objects, as well as the effect of refraction.

For most surfaces, the incident light ray will be reflected into a spread of directions resulting in an outgoing light distribution or lobe, depending on the incident angle. This behavior is described by the so-called BRDF (bidirectional reflectance distribution function [17]). In order to visualize this distribution we provide images captured perpendicular to the plane of reflection. The accompanying video shows the resulting distributions from different viewpoints.

In the following images we will occasionally superimpose intensity iso-lines into the images, to visualize the intensity gradient in the light distributions, e.g. in BRDF lobes, (Figure 3).

4.1 Mirror Reflection

For a perfectly mirroring sphere (leftmost column of Figure 3) the incident light ray is reflected into the mirror direction according to the surface normal. The angle between the incident ray and the reflected ray equals two times the angle between the incident ray and the normal.

4.2 Glossy Reflection

Rather than reflecting a single ray the silver paint in the second column reflects the incoming ray into a distribution of directions mainly centered around the mirror direction, the so-called glossy lobe. This glossy reflection is caused by rough specular surfaces or, as in our case by a clear paint containing mirroring particles at random orientations.

4.3 Diffuse Reflection

In the simplest case of a diffuse surface the incident light is reflected into a very broad lobe that is always centered around the surface normal independent of the incident direction (third column of Figure 3). Light is equally scattered into all directions. The profile of the lobe is given by the irradiance each voxel receives from the diffuse/Lambertian reflection. While the reflected radiance is equal in all directions, the irradiance is affected by the area foreshortening of the illuminated patch viewed from the voxel. As a result, we obtain a cosine weighted lobe

which is invisible at grazing angles and always centered around the surface normal.

4.4 Diffuse + Glossy Reflection

The last column of Figure 3 shows a diffuse blue sphere covered with a transparent, glossy varnish. In the iso-line plot of the second row the coexistence of a diffuse and a specular lobe is visible.

4.5 Anisotropic Reflection

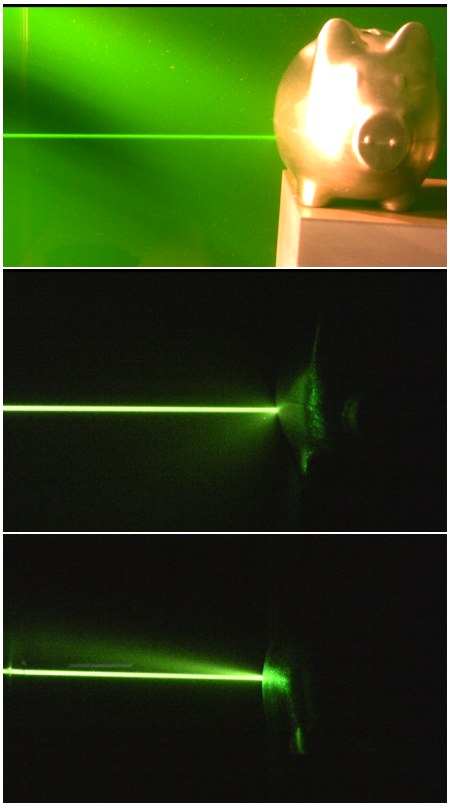

Figure 4: Front and top view of the anisotropic reflections of a brushed metal piglet. The reflected glossy lobe is broad vertically but rather sharp when viewed from the top.

While the diffuse and specular lobes seen before are almost rotationally symmetric around the mirror direction, anisotropic BRDFs have a preferred reflection direction caused by oriented surface features, such as grooves or scratches, see Figure 4. The width of the resulting glossy lobe varies with their orientation. As a consequence, anisotropic reflections change when the surface is rotated around its normal. The distorted shape of an anisotropic lobe can be easily explored in 3D while it is hard to visualize the anisotropy in a 2D projection.

4.6 Transparency vs. Translucency

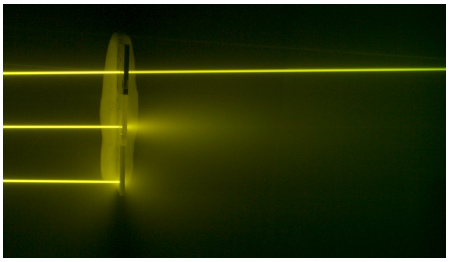

Figure 5: Light transmission through transparent (top) and translucent materials of different optical density (center and bottom).

So far, we have investigated opaque surfaces where the incident light is reflected. Instead of being reflected, light incident on transparent or translucent materials is partially transmitted. Light goes straight through a planar transparent sheet if illuminated perpendicularly. Due to absorption the intensity of light might be reduced, see Figure 5.

Inside a translucent material, scattering widens the transmitted beam. The width of the transmitted lobe depends on the scattering density and the phase function of the material. This effect is described by the BTDF (bidirectional transmittance distribution function). The subsurface scattering inside translucent materials further leads to the effect that light incident at one point might leave the object at some other location (BSSRDF – bidirectional scattering-surface reflectance distribution function [17]). As a result, one can observe the glow emitted from any surface point of the bottom slab in Figure 5.

4.7 Refraction

As soon as light enters a medium with a different index of refraction, hitting the surface under some angle, the light ray will be refracted. In Figure 6,

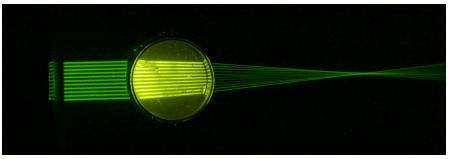

Figure 6: Refraction by cylinder filled with glycerol.

the fan of parallel incident light rays changes directions on the first and the second interface between water outside and the glycerol inside the cylinder. The light rays inside a medium of constant index of refraction remain straight.

4.8 Continuous Refraction – Mirages

At the interface between two fluids with different index of refraction – in our case water and glycerol – there will be a region, where the index changes gradually, with the gradient pointing downwards. In this region, a light ray approaching the interface from the denser medium is continuously refracted into the direction of the gradient. The light ray therefore is curved and will point downwards after some point. This effect of superior mirages is visualized in Figure 1. With a set of rays we demonstrate the typical inversion of the image reflected by a mirage. If the interface would feature a sharp transition, one would observe total internal reflection with straight rather than curved rays.

5 Lenses

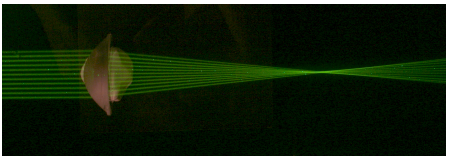

Figure 7: Refraction due to a convex lens.

The effect of a focusing lens is demonstrated using a grid of parallel incoming rays in Figure 7. The convergence to the focal point and the hour-glass shape of the ray bundle can nicely be observed in 3D.

Please note, that the index of refraction of the fluid is much larger compared to air such that the focal length of lenses is increased.

5.1 Astigmatism

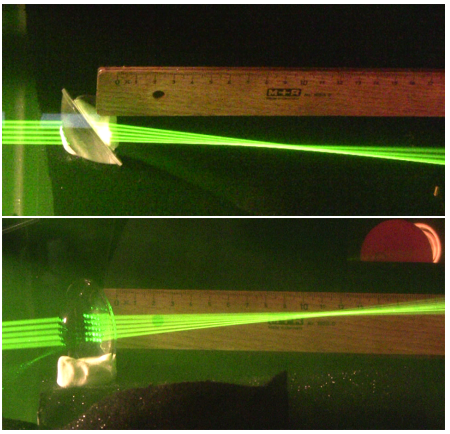

Figure 8: Top and side view of an astigmatic focus. The focal point moves from 9.5 cm horizontally to 11.5 cm vertically.

Figure 8 depicts the configuration of rays caused by a tilted lens illuminated with a regular grid of 5×5 parallel rays. In our configuration and for astigmatic lenses the focal length along the vertical axis of the lens is different from the horizontal focal length. This complex spatial arrangement is clearly visible in the two different views. It is far less intuitive trying to observe this behavior using a planar reflector screen.

5.2 Comatic Aberration

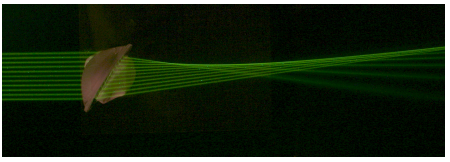

Figure 9: Off-axis distortion caused by comatic aberration due to an imperfect lens.

Coma or comatic aberration is the effect of a lens exhibiting different focal points depending on where the light ray intersects the lens. In our case (Figure 9) the focal length increases from top to bottom, resulting in this very particular wedge shaped caustic.

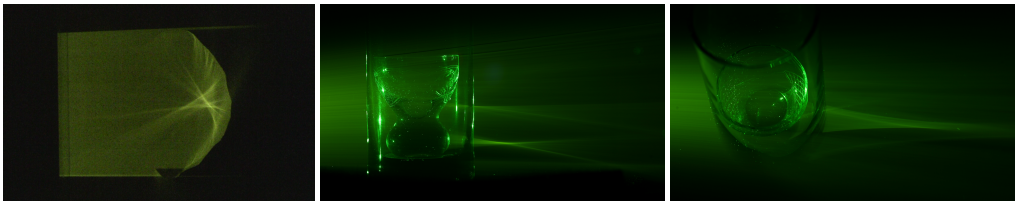

Figure 10: Reflective (left) and refractive (middle, right) caustics. The shape of the glass creates complex volumetric caustics whose 3D structure is only revealed viewing it from different directions.

5.3 Caustics

A caustic is an accumulation of light rays produced by the reflection or refraction through curved surfaces.

The geometric structure of the caustics heavily depends on the incident light distribution and the geometry of the object creating the caustic. As the reflections and refractions do not necessarily lie in a plane and therefore form complex 3D structures, their beauty can best be appreciated if viewed inside a volume as seen in Figure 10.

5.4 Diffraction

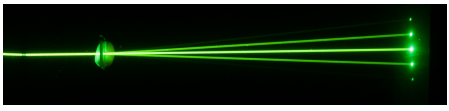

Figure 11: Diffraction due to a diffraction grating.

Another mechanism that causes bending of light rays is diffraction on small-scale obstacles. In Figure 11, the laser beam hits a grating consisting of fine, regularly spaced lines. In the resulting diffraction pattern, one sees how the incident beam is split into a symmetric fan of rays. The 0th-order beam still carries most of the energy while higher orders of diffraction exhibit smaller radiance.

6 Global Light Transport

6.1 Structure of a Light Field

The next experiment shows how an incident plane of light intersects the transparent front piece of a bike light. The form of the front glass contains a focussing lens in the middle which is surrounded by ripples, acting as an array of weak small lenses in this one-dimensional illumination. In the captured image (Figure 12), one sees how the resulting light field changes with distance to the glass piece. In the near-field a set of separate rays around the central beam are visible. The individual beams become more and more blurred and blend into each other in the far-field.

6.2 Interreflections

As a last example, we show the light transport due to interreflections between a mirroring, glossy and a diffuse surface. The mirrored illumination ray and the secondary glossy reflection in Figure 13 are still clearly visible. The tertiary diffuse reflection however is hardly distinguishable. It shows the limit of our method. Here, the light scattered from the second, glossy bounce is so strong and so spread out that any further reflection does contribute very little. This changes if an additional occluder is introduced into the scene. The dynamic range of the scene is still large.

7 Discussion

7.1 Limitations

As we use the optical path to observe light transport, there are some principled limitations to the presented method. The fluorescence transforms the originally incident wavelength, therefore, we can only usefully employ a single input wavelength, and thus cannot study any color effect.

Further, while we can qualitatively observe scattering on object surfaces, a quantitative measurement is difficult: surface reflectance models are usually expressed for light interaction in vacuum, for which air is usually a sufficient approximation when measuring. The water we submerge the scene in

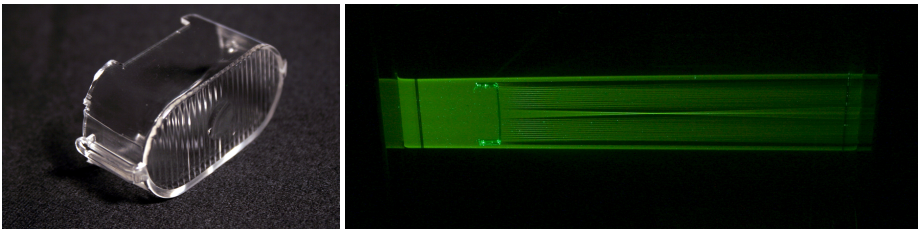

Figure 12: Near-field and far-field caused by a complex optical element.

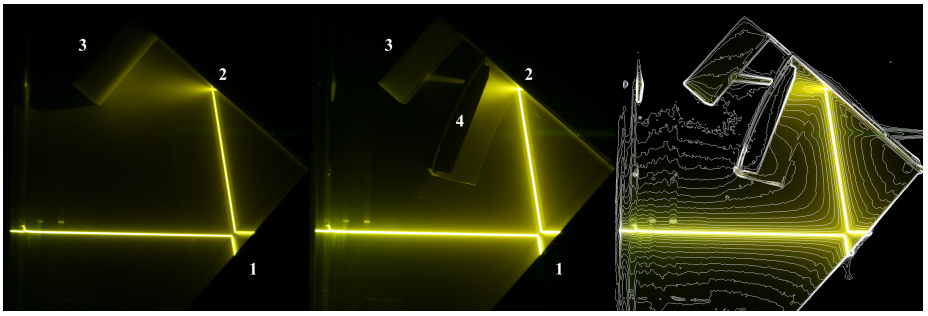

unoccluded transport occluder inserted superimposed iso-lines

Figure 13: Interreflection - from a mirroring surface (1), onto a glossy surface (2) onto a diffuse reflector (3). The third bounce is so weak that it is only visible if a partial occluder (4) is inserted.

has, however, a distinctively different index of refraction, and, accordingly, the scattering processes – such as Fresnel reflection – are substantially influenced.

An additional restriction is posed by the distribution of the fluorescent dye. While it is simple to achieve a homogeneous distribution of the dye inside the immersing fluid, we cannot easily dye solid transparent objects. Thus, the light transport inside them is difficult to observe.

7.2 Advanced Effects

There are advanced optical effects which are not often simulated in computer graphics. These include effects introduced by crystalline structures [9]. Crystals exhibit double (uni-axial crystals) or triple refraction (bi-axial crystals), known as birefringence and trirefringence, respectively. Another subtle optical effect of crystal optics is conical refraction [1]. Using the proposed setup, it might be possible to study these effects and evaluate their potential or irrelevance for realistic image synthesis. It might also be possible to study polarization-based effects by placing a polarization filter in front of the light source and observing the changing intensity when rotating the filter. This way, a more intuitive understanding of advanced optical effects might be developed by students and researchers alike.

7.3 Conclusion

In this article, we have presented a simple setup for the real-world visualization of light transport effects. As it provides the means to explore light-matter interaction with the human visual sense, it enables ample opportunities for experimentation even for non-experts. Due to its simple and inexpensive nature and its ability to visualize a wide variety of optical phenomena, we imagine our setup to be a valuable tool for educational purposes and the study of complex light interaction.

In the future, related methods might lead to integrated measurement techniques for both surface geometry and reflectance. In the meantime, we hope to have contributed towards a better understanding of light transport in the real world.

8 Acknowledgements

This work has been partially funded by the DFG Emmy Noether fellowship (Le 1341/1-1) and the Max Planck Center for Visual Computing and Communication (BMBF-FKZ01IMC01). Ivo Ihrke was supported by a Feodor Lynen fellowship of the Humboldt Foundation.

References

[1] Max Born and Emil Wolf. *Principles of Optics*. Cambridge University Press, 7 edition, 1999.

[2] S. Deusch and T. Dracos. Time-Resolved 3D Passive Scalar Concentration-Field Imaging by Laser Induced Fluorescence (LIF) in Moving Liquids. *Meas. Sci. Technol.*, 12:188–200, 2001.

[3] Frédo Durand, Nicolas Holzschuch, Cyril Soler, Eric Chan, and François X. Sillion. A Frequency Analysis of Light Transport. *ACM Transactions on Graphics (Proc. SIGGRAPH)*, 24(3):1115–1126, August 2005.

[4] James Foley, Andries van Dam, Steven Feiner, and John Hughes. *Computer Graphics: Principles and Practice, second edition*. Addison-Wesley Professional, 1990.

[5] Gaurav Garg, Eino-Ville Talvala, Marc Levoy, and Hendrik P. A. Lensch. Symmetric Photography: Exploiting Data-Sparseness in Reflectance Fields. In *Rendering Techniques 2006 (Proc. EGSR)*, pages 251–262, June 2006.

[6] Abhijeet Ghosh, Shruthi Achutha, Wolfgang Heidrich, and Matthew O'Toole. BRDF Acquisition with Basis Illumination. In *IEEE International Conference on Computer Vision (Proc. ICCV)*, 2007.

[7] Donald A. Glaser. Some Effects of Ionizing Radiation on the Formation of Bubbles in Liquids. *Phys. Rev.*, 87(4):665–665, 1952.

[8] Andrew Glassner. *Principles of Digital Image Synthesis*. Morgan Kaufmann, 1995.

[9] Stephane Guy and Cyril Soler. Graphics Gems Revisited: Fast and Physically-Based Rendering of Gemstones. *ACM Transactions on Graphics (Proc. SIGGRAPH)*, 23(3):231–238, August 2004.

[10] Tim Hawkins, Per Einarsson, and Paul Debevec. A Dual Light Stage. In *Rendering Techniques 2005 (Proc. EGSR)*, pages 91–98, June 2005.

[11] Tim Hawkins, Per Einarsson, and Paul Debevec. Acquisition of Time-Varying Participating Media. *ACM Transactions on Graphics (Proc. SIGGRAPH)*, 24(3):812–815, 2005.

[12] Matthias B. Hullin, Martin Fuchs, Ivo Ihrke, Hans-Peter Seidel, and Hendrik P. A. Lensch. Fluorescent Immersion Range Scanning. *ACM Transactions on Graphics (Proc. SIGGRAPH)*, 26(3), 2008. (to appear).

[13] Dhruv Mahajan, Ira Kemelmacher Shlizerman, Ravi Ramamoorthi, and Peter Belhumeur. A Theory of Locally Low Dimensional Light Transport. *ACM Transactions on Graphics (Proc. SIGGRAPH)*, 26(3):62:1–62:10, July 2007.

[14] S. K. Nayar, G. Krishnan, M. D. Grossberg, and R. Raskar. Fast Separation of Direct and Global Components of a Scene Using High Frequency Illumination. *ACM Transactions on Graphics (Proc. SIGGRAPH)*, 25(3):935–944, 2006.

[15] Addy Ngan, Frédo Durand, and Wojciech Matusik. Experimental Analysis of BRDF Models. In *Rendering Techniques 2005 (Proc. EGSR)*, pages 117–126, 2005.

[16] Addy Ngan, Frédo Durand, and Wojciech Matusik. Image-Driven Navigation of Analytical BRDF Models. *Rendering Techniques 2006 (Proc. EGSR)*, pages 399–407, 2006.

[17] F. Nicodemus, J. Richmond, J. Hsia, J. Ginsberg, and T. Limberis. *Geometric Considerations and Nomenclature for Reflectance*. Monograph 161. National Bureau of Standards (US), oct 1977.

[18] Peter Shirley and R. Keith Morley. *Realistic Ray Tracing*. A. K. Peters, Ltd., Natick, MA, USA, 2003.

[19] Gregory J. Ward. Measuring and Modeling Anisotropic Reflection. *Proc. ACM SIGGRAPH '92*, 26(2):265–272, July 1992.

[20] Turner Whitted. An Improved Illumination Model for Shaded Display. *ACM Communications*, 23(6):343–349, June 1980.